# Bitter Taste Receptor Agonists Alter Mitochondrial Function and Induce Autophagy in Airway Smooth Muscle Cells

Shi Pan, Pawan Sharma[#], Sushrut D. Shah, and Deepak A. Deshpande[*]

Center for Translational Medicine, Jane and Leonard Korman Lung Center, Thomas Jefferson University, Philadelphia, PA

[*]Address for Correspondence:
Deepak A. Deshpande, Ph.D.
Associate Professor,
Center for Translational Medicine,
Jeff Alumni Hall, Rm 543,
1020 Locust Street,
Philadelphia, PA 19107.
Phone: 215-955-3305
Fax: 215-503-5731
E-mail: deepak.deshpande@jefferson.edu

**Running Title** Mitochondria in ASM cell death

**Keywords**: Asthma, GPCR, TAS2R, mitochondria

**Abstract**

Airway remodeling including increased airway smooth muscle (ASM) mass is a hallmark feature of asthma and COPD. We previously identified the expression of bitter taste receptors (TAS2Rs) on human ASM cells, and demonstrated that known TAS2R agonists could promote ASM relaxation and bronchodilation, and inhibit mitogen-induced ASM growth. In this study we explored cellular mechanisms mediating the anti-mitogenic effect of TAS2R agonists on human ASM cells. Pre-treatment of ASM cells with TAS2R agonists, chloroquine and quinine, resulted in inhibition of cell survival, which was largely reversed by bafilomycin A1. Transmission electron microscope studies demonstrated the presence of double-membrane autophagosomes and deformed mitochondria. In ASM cells, TAS2R agonists decreased mitochondrial membrane potential, increased mitochondrial ROS and mitochondrial fragmentation. Inhibiting dynamin-like protein (DLP1) reversed TAS2R agonist-induced mitochondrial membrane potential change, and attenuated mitochondrial fragmentation and cell death. Consistent with these findings, the expression of mitochondrial protein BCL2/adenovirus E1B 19 kDa protein-interacting protein 3 (Bnip3) and mitochondrial localization of DLP1 were significantly up-regulated by TAS2R agonists. More importantly, inhibiting Bnip3 mitochondrial localization by dominant-negative Bnip3 significantly attenuated cell death induced by TAS2R agonist. Collectively, TAS2R agonists, chloroquine and quinine modulate mitochondrial structure and function resulting in ASM cell death. Furthermore, Bnip3 plays a central role in TAS2R agonist-induced ASM functional changes via a mitochondrial pathway. These findings further establish the cellular mechanisms of anti-mitogenic effects of TAS2R agonists, and identify a novel class of receptors and pathways that can be targeted to mitigate airway remodeling as well as bronchoconstriction in obstructive airway diseases.

## INTRODUCTION

Airway inflammatory diseases such as asthma and COPD are characterized by inflammation, mucus production, airway remodeling and hyperresponsiveness resulting in severe bronchoconstriction (4, 27, 45). The chronic nature of these diseases leads to structural and functional changes in resident cells of the airway wall including ASM cells (27, 28, 39, 40). Histological evaluation of asthmatic lung samples reveals a significant increase in the ASM mass (8, 17, 19, 25), which is correlated with asthma severity (2, 15, 55). Alterations in ASM mass and phenotype are now appreciated as pathogenic mechanisms of obstructive lung diseases (6).

G protein-coupled receptor (GPCR) signaling plays a vital role in the regulation of ASM contraction, relaxation, and proliferation (4, 10) and therefore, agonists/antagonists of GPCRs represent potentially efficacious anti-asthma medications. Current anti-asthma therapies, including beta-agonists and corticosteroids, aim at alleviating bronchoconstriction and inflammation, respectively, but have a very limited effect on remodeling (4). Thus there is a pressing need for identifying new drugs that cause both ASM relaxation and inhibition of growth.

Recently we identified the expression of type II taste receptors (TAS2Rs) on human ASM cells and characterized intracellular signaling mediated via these receptors using a panel of known TAS2R agonists (12, 50). Among the 25 known taste receptors at least three subtypes are highly expressed (T2R10, T2R14, T2R31) and three more are moderately expressed (T2R5, T2R4, T2R19) in human ASM. Expression of TAS2Rs on guinea pig and murine ASM has also been demonstrated recently (34, 47). Extant TAS2R agonists include both synthetic and natural compounds. One group includes chloroquine and quinine, which activate T2R10, T2R14, and T2R31 expressed on human ASM cells (12, 35). Stimulation of ASM cells with TAS2R agonists

resulted in an increase in intracellular calcium that was Gβγ–, PLC- and $IP_3$-dependent. Interestingly, elevation of calcium upon TASR stimulation was associated with a robust relaxation of ASM cells and airway rings. This relaxation effect of TAS2R agonists was confirmed by three independent laboratories using mouse, guinea pig and human airways (12, 34, 47). Studies using lung slices (human and murine) and *in vivo* aerosol challenge in murine models have demonstrated efficacious bronchodilation by TAS2R agonists. These observations posit TAS2R agonists as a new class of bronchodilators for clinical use. Recent study from our laboratory demonstrated that TAS2R agonists such as chloroquine and quinine inhibit mitogen-induced human ASM growth (50). Furthermore, the anti-mitogenic effect of TAS2R agonist is mediated, at least partially, via inhibition of PI3 kinase pathway and arresting of cell cycle progression (50).

Increases in ASM mass could result from multiple mechanisms including an increase in cell number (hyperplasia), size (hypertrophy), epithelial to mesenchymal transition (EMT), or decrease in cell death. Inhibition of ASM growth by anti-mitogenic agents can occur via targeting of any of these mechanisms including autophagy and mitochondrial-initiated cell death. In this study we aimed to determine additional cellular mechanisms involved in the anti-mitogenic effect of TAS2R agonists, chloroquine and quinine on human ASM cells. Using advanced microscopic imaging and biochemical tools herein we demonstrate that TAS2R agonists modulate mitochondria dynamics and function leading to ASM cell death. Chloroquine- and quinine-induced ASM cell death was reversed by pre-treating cells with befilomycin A1, an autophagy inhibitor, suggesting the role of autophagy. Interestingly, the anti-mitogenic effect of TAS2R agonists on human ASM cells was attenuated by inhibiting Bnip3, a mitochondrial protein, using dominant negative Bnip3 or a DLP1 inhibitor Mdivi-1, suggesting a central role

for mitochondrial protein Bnip3 and autophagy in TAS2R agonist-mediated anti-mitogenic effect on human ASM.

## METHODS

### *Materials*

Antibodies against Mfn1, Mfn2, and Bnip3 were from Abcam (Burlinggame, CA, USA). DLP1 and Opa1 antibodies were from BD Bioscience (Franklin Lakes, NJ, USA). VDAC, Beclin-1 and ATG-5 antibody were purchased from Cell Signaling Technology (Beverly, MA, USA). IRDye 680 or 800 secondary antibodies were from Rockland (Gilbertsville, PA, USA). Quantitative PCR arrays and SYBR green reagents were purchased from Qiagen (Valencia, CA, USA). MTT cell proliferation assay kit, MitoTracker Green and MitoSox red are from Thermo Fisher Scientific (Pittsburg, PA, USA). siRNA oligos were obtained from Dharmacon (Lafayette, CO, USA). Rabbit-anti LC3-β, anti-β-actin, Bafilomycin A1 (Baf A1), 3-Methyl adenine (3-MA), chloroquine, quinine, saccharine, and other reagents were obtained from Sigma (St. Louis, MO, USA) or from previously identified sources (12, 50). Wild type and dominant-negative Bnip3 adeno-associated virus were from ViGene Bioscience (Rockville, MD, USA)

### *Cell culture*

Human ASM cultures were established from human tracheae or primary bronchi using enzyme dissociation method, and were grown in F-12 medium with supplements as described previously (11, 12, 37). ASM cells in subculture during the second through fifth cell passages were used. The cells were maintained in F-12 medium with no serum and supplemented with 1% insulin transferrin selenium (arresting medium) for 24-48 h before the experiments.

### *Isolation of mitochondria*

Mitochondria were isolated from ASM cells after the treatments with TAS2R agonists using Mitochondria Isolation Kit (Miltenyi Biotec) (21, 36). Briefly, $1x10^7$ ASM cells were collected, washed with PBS and resuspended in 1 ml lysis buffer. Cell homogenates were prepared using a dounce homogenizer and incubated with 50 µl of anti-Tom22 coated beads for 1 h with gentle shaking at 4°C. After the non-specific binding was washed out in the magnetic field, mitochondria were isolated for analysis.

*siRNA transfection and viral (Adeno-Associated Virus, AAV) infection*

siRNA transfection was performed in human ASM cells as described previously (49). Briefly, cells were seeded in 6-well plates one day before transfection. Transfection mixture was prepared by adding 2-5 µl of 5 µM siRNA and 5 µl DharmaFECT1 (GE Healthcare) reagent to serum-free medium. After incubating at room temperature for 20 min the mixture was transferred to a new tube containing 1 ml of complete medium (final siRNA concentration was 25 nM) and transferred to cells after 5 min. AAV infection was performed according to the manufacturer's instruction (ViGene Bioscience). Briefly, cells were seeded on a 6-well plate one day before the infection. On the following day, cells were infected with $10^5$/cell AAV particles expressing either wild type or dominant-negative (DN) Bnip3. After 12 h incubation, virus-containing media was replaced with regular culture media. The success in infection was monitored by green fluorescence protein (GFP) expression using a fluorescence microscope. For confocal studies, cells were cultured on confocal dishes, serum starved and treated with TAS2R agonists for 24 h before propidium iodide (PI) staining was performed.

*Propidium iodide (PI) staining*

Human ASM cells were incubated with 4 μl of PI (10 mg/ml) in 1 ml of medium in a $CO_2$ incubator. The staining solution was removed after 5 min followed by three washes with PBS. ASM cell images were acquired using a confocal ($\lambda_{ex}$ 535 nm, $\lambda_{em}$ 617 nm) microscope.

*MTT and CyQuant assay*

MTT and CyQuant assays were performed as described previously (50). Human ASM cells were grown to sub-confluence in 96-well cell culture plates before switching to growth arrest media for 24 h (F12 + 1% ITS) and then treated with TAS2R agonists in the presence or absence of PDGF (10 ng/ml) for 24 h. In some cases cells were pretreated with 3 μM Mdivi-1 for 2 h before treating with TAS2R agonists ± PDGF. At the end of the treatment, media was removed and cells incubated with MTT or CyQuant reagent for 4 h or 1 h respectively, and absorbance or fluorescence determined using a plate reader.

*Immunostaining and light microscope imaging*

Cells were plated onto pre-cleared glass coverslips in 6-well culture dishes and fixed for 15 min at 4°C in 3% paraformaldehyde (PFA) and then permeabilized by incubation for 5 min at 4°C using 3% PFA and 0.3% Triton X-100. Fixed cells were first blocked for 2 h at room temperature in cyto-TBS buffer containing 1% BSA and 2% normal donkey serum. Incubation with primary antibody rabbit anti-LC3βII (1:100) occurred overnight at 4°C in cyto-TBST followed by FITC-conjugated secondary antibody. For negative controls, cells were incubated with either isotype-matched mouse IgG or rabbit antiserum. Coverslips were mounted using ProLong antifade medium (Molecular Probes, Inc. USA). Fluorescent imaging of LC3 was performed by capturing a mid-cell section of 0.3 μm focal depth using an Olympus LX-70 FluoView Confocal Laser Scanning Microscope (Olympus America Inc, Melville, N.Y.)

equipped with a 40x objective. Brightfield images were acquired to assess the morphology of the cell with treatment protocol.

*Electron microscopy (EM) studies*

The ultrastructural details of the cell were assessed using transmission electron microscopy (TEM) to measure autophagosome formation and assess mitochondrial integrity (46). Cells were grown in 6-well culture plates, treated as described above and processed further for Transmission Electron Microscopy. Imaging was performed at the core facility at University of Maryland, Baltimore using FEI Tecnai T12 high-resolution microscope.

*Western blotting*

Western blotting (immunoblotting) was performed as described previously (42, 43). The images were acquired by Odessey image scanner (LiCor). Equal loading of protein was ensured by determining the expression of β-actin or tubulin.

*RNA isolation, RT-PCR and Real-Time PCR array*

Cells grown on 6-well plates were treated with PDGF or vehicle with or without pretreatment with TAS2R agonists for 24 h, and total RNA was harvested as described in our previous studies (37, 50). Total RNA (1 μg) was converted to cDNA by RT reaction and the reaction stopped by heating the samples at 94$^{o}$C for 5 min. Quantitative real-time PCR was performed using RT$^{2}$ Profiler PCR Array for mitochondria genes (PAHS-087Z) using Applied Biosystems real time PCR machine (Mx3005). Raw Ct values were obtained using software recommended threshold fluorescence intensity. Gene expression data was calculated as described previously using expression of internal control gene (GAPDH) (12, 49).

*Assessment of Mitochondrial Membrane Potential and Reactive Oxygen Species (ROS) generation*

Mitochondrial membrane potential and ROS measurements were performed as described previously (43). Briefly, after the treatment with TAS2R agonists, ASM cells were incubated with mitochondrial membrane potential dye Tetramethylrhodamine, ethyl ester (TMRE) or mitochondrial ROS probe MitoSox red for 30 min, then washed with PBS to remove the unincorporated dyes. Mitochondrial membrane potential and ROS generation were monitored by live-cell imaging using a confocal microscope. Mitochondria images were acquired by Fluoview (Olympus) using a 60x Oil objective and analyzed using NIH ImageJ 1.44 software.

*Statistical analyses*

Data are presented as mean ± SEM values from at least three experiments, in which each experiment was performed using a different ASM culture derived from a unique donor. Individual data points from a single experiment were calculated as the mean value from three replicate observations, and reported as fold change from vehicle treated group. Statistically significant differences among groups were assessed by either student t-test or ANOVA using Prism Graphpad software (Graphpad, La Jolla, CA, USA), with values of $p<0.05$ sufficient to reject the null hypothesis.

## RESULTS

### *TAS2R agonists induce ASM cell death*

We used PDGF to induce ASM growth and determined the effect of three different TAS2R agonists chloroquine (Chloro), quinine (Quin) and saccharin (Sacc) on mitogen-induced ASM growth. ASM cell survival was significantly decreased by chloroquine and quinine (Figure 1A) supporting the anti-mitogenic effect of TAS2R agonists on human ASM cells (50). Saccharine, a relatively weak TAS2R agonist, caused a modest inhibition of ASM growth that was not statistically different from vehicle-pretreated control. Further, human ASM cells were pre-treated with autophagy inhibitor, Baf A1, followed by TAS2R agonists. Baf A1 mitigated cell death-inducing effect of chloroquine and quinine on human ASM cells (Figure 1A-B) suggesting a potential role of autophagy. Induction of autophagy in human ASM by chloroquine and quinine was further confirmed by immunofluorescence and immunoblot detection of LC3β puncta formation and LC3β II accumulation, respectively. LC3β accumulation in human ASM cells was significantly reduced in the presence of Baf A1 and 3-methyl adenine (3MA) (Figure 1C and 1D). Transmission electron microscopy revealed accumulation of double-membrane autophagosomes, vesicles and deformed mitochondria in human ASM cells upon treatment with TAS2R agonists, chloroquine and quinine in the presence of PDGF (Figure 1E). Collectively, these findings suggest the involvement of autophagy in TAS2R agonist-mediated anti-mitogenic effect on human ASM cells.

### *TAS2R agonists impair mitochondrial function in human ASM cells*

Our TEM studies demonstrated that chronic treatment of human ASM cells with TAS2R agonists increased accumulation of deformed mitochondria (Figure 1E). Therefore, we next assessed whether mitochondrial function was altered by TAS2R agonists. Indeed, the

mitochondrial membrane potential was significantly decreased after exposure to TAS2R agonists compared to vehicle treated cells (4078.89±255.77, chloro+PDGF; 16389.80±973.86, quin+PDGF; and 44871.11±1159.62 vehicle controls; $p<0.05$, n=9) (Figure 2A). Because mitochondrial membrane potential is the primary drive for ATP synthesis (13, 24), we further examined cellular ATP levels in ASM cells exposed to chloroquine and quinine. TAS2R agonists significantly decreased cellular ATP levels compared to vehicle-treated controls (0.62±0.03 fold basal for chloro+PDGF; and 0.74±0.14 fold basal for quin+PDGF; $p<0.05$, n=3) (Figure 2B). Further, mitochondrial ROS levels in human ASM cells were significantly increased by TAS2R agonists (5128.66±104.51 chloro+PDGF; 2982.24±254.28 quin+PDGF; and 2467.8±356.44 vehicle-treated controls; n=24, $p<0.05$) (Figure 2C). Collectively, these data strongly suggest that chronic exposure of human ASM cells to TAS2R agonists, chloroquine or quinine results in mitochondrial dysfunction as indicated by a significant decrease in mitochondrial membrane potential, cellular ATP levels, and a significant increase in mitochondrial ROS.

***TAS2R agonists increase mitochondrial fragmentation in human ASM cells***

To further understand the subcellular effect of TAS2R agonists in human ASM cells, we determined the effect of chloroquine and quinine on mitochondrial dynamics. In control cells exposed to vehicle, mitochondria were interconnected and formed tubular and granular network. Exposure of cells to TAS2R agonists caused an increase in fragmented mitochondria as determined by live-cell confocal imaging (Figure 3A). The mitochondrial morphology data were further analyzed quantitatively using form factor (an indicator of mitochondria branching) and aspect ratio (an indicator of mitochondria length). Chloroquine and quinine significantly increased mitochondrial fragmentation (Figure 3A-C). The mitochondrial branches were significantly decreased by the exposure of ASM cells to chloroquine plus PDGF (2.40±0.08,

n=5, $p<0.05$) or quinine plus PDGF (2.26±0.08, n=5, $p<0.05$) compared to vehicle control (3.92±0.19) (Figure 3B). Similarly, compared to vehicle control (3.89±0.15), chloroquine or quinine plus PDGF significantly decreased length of mitochondria (2.1±0.06 and 2.65±0.09 respectively, n=5, $p<0.05$) (Figure 3C). Interestingly, exposure of human ASM cells to TAS2R agonists did not significantly change expression levels of mitochondrial dynamics proteins including dynamin-like protein 1 (DLP1), optic atrophy 1 (Opa1), mitofusin 1 (Mfn1) and mitofusin 2 (Mfn2) indicating the alteration in mitochondrial dynamics is not due to the changes in the expression levels of the mitochondrial dynamic proteins (Figure 3D). These data suggest that chronic exposure of human ASM cells to chloroquine and quinine alters mitochondrial dynamics leading to mitochondrial fragmentation.

***TAS2R agonists increase Bnip3 expression and DLP1 mitochondrial localization in human ASM cells***

To determine the molecular mechanisms by which chloroquine and quinine change mitochondrial dynamics and function, we performed $RT^2$ profiler PCR Array analysis (Figure 4). Real-time PCR analysis revealed significant upregulation of Bnip3 expression in human ASM cells exposed to chloroquine and quinine (1.59±0.05 and 2.41±0.07 fold control, chloro or quin+PDGF respectively; $p<0.05$, n=4) (Figure 4A-B).

To explore the molecular mechanisms by which chloroquine and quinine alter mitochondria morphology and function, we isolated mitochondria from human ASM cells exposed to TAS2R agonists. Western blotting of lysates from isolated mitochondria demonstrated significantly increased levels of DLP1 in the mitochondrial fraction upon treatment with chloroquine or quinine plus PDGF compared to vehicle controls (Figure 4C-D). There was no significant change in the protein levels of other mitochondrial proteins such as (voltage-

dependent anion channel) VDAC (Figure 4C bottom panel). Other studies have demonstrated that Bnip3 increases DLP1 in mitochondria (29). Our data support a model in which TAS2R agonists up-regulate Bnip3 expression, which increases DLP1 levels in mitochondria resulting in mitochondrial fragmentation and dysfunction.

***Bnip3 siRNA partly reverses TAS2R agonists-induced mitochondrial fragmentation***

To confirm the role of Bnip3 in TAS2R-induced mitochondrial fragmentation, we down-regulated Bnip3 in human ASM cells using a siRNA approach. Transfection of human ASM cells with Bnip3 siRNA significantly decreased Bnip3 levels without affecting other mitochondrial proteins such as Opa1 (Figure 5A-B). More importantly, transfection with Bnip3 siRNA partly reversed mitochondrial fragmentation induced by chloroquine or quinine plus PDGF, as indicated by confocal imaging as well as the analysis of form factors and aspect ratio (Figures 5C-E). In Bnip3 siRNA transfected human ASM cells, mitochondrial branches and length were significantly increased compared to control siRNA transfected cells (Figure 5C-E). Down-regulation of Bnip3 expression by siRNA did not have significant effects on the protein levels of DLP1 (data not shown). These data strongly suggest that Bnip3 plays a role in TAS2R agonists-induced mitochondrial fragmentation. However, current siRNA/shRNA approaches (that work in primary ASM) are not amenable to analyses of ASM growth and we were not able to demonstrate the role of Bnip3 in the regulation of ASM growth by TAS2R agonists. Therefore, we used additional approaches to down-regulate mitochondrial Bnip3 levels.

***Dominant-negative Bnip3 inhibits TAS2R agonists-induced cell death in human ASM cells***

We have demonstrated that TAS2R agonists-induced increase in mitochondrial fragmentation and cell death in human ASM cells is associated with increased Bnip3 expression. To further understand the role of Bnip3 in TAS2R agonists-induced mitochondrial fragmentation

and cell death in ASM cells, we generated adeno-associated virus (AAV) expressing wild type (WT) or dominant-negative (DN) Bnip3 lacking the c-terminal mitochondrial localization domain. The truncated Bnip3 does not localize to mitochondria, and functions as the dominant-negative form of Bnip3. The infection efficiency was determined by GFP-fluorescence (Figure 6A). The expression of WT and DN Bnip3 was confirmed by western blotting (Figure 6B). Using this approach, we determined the role of Bnip3 in TAS2R agonists-induced cell death in Bnip3 expressing human ASM cells (Figure 6C). TAS2R agonists-induced cell death was significantly decreased in human ASM cells transfected with DN-Bnip3 compared to cells transfected with WT-Bnip3 (a 66% decrease in chloro+PDGF group and a 73% decrease in quin+PDGF group, n=4; $p<0.01$ for both). These findings demonstrate that TAS2R agonists-induced ASM cell death is mediated via Bnip3 localization to mitochondria and mitochondrial mechanisms.

***Inhibition of mitochondrial fission by DLP1 inhibitor Mdivi-1 attenuates TAS2R agonists-induced mitochondrial fragmentation, decrease in mitochondrial membrane potential, and cell death in human ASM cells***

Our data suggest that chronic exposure of human ASM cells to TAS2R agonists increases mitochondrial fragmentation. Because excessive mitochondrial fission causes mitochondrial depolarization and cell death (58), (23), we hypothesized that inhibition of mitochondrial fission using DLP1 inhibitor, Mdivi-1, would rescue loss of mitochondrial functions and cell death induced by TAS2R agonists. Pre-incubation of ASM cells with 3 μM Mdivi-1 for 2 h, a well-established inhibitor of DLP1, decreased chloroquine- and quinine- induced mitochondrial fragmentation (Figure 7A). Mdivi-1 pre-treatment significantly reversed the decrease in mitochondrial membrane potential induced by TAS2R agonists (69% increase vs chloro+PDGF;

and 62.1% increase vs quin+PDGF; n=10; $p<0.05$ for both) (Figure 7B). Further, pretreatment with Mdivi-1 significantly decreased TAS2R agonists-induced cell death (Figure 7C-D) (30% increase in cell survival vs chloro+PDGF; and 35.4% increase vs quin+PDGF; n=3, $p<0.05$ for both) (Figure 7D). These data suggest that TAS2R agonists increase mitochondrial DLP1 accumulation leading to mitochondrial fragmentation and cell death.

**DISCUSSION**

In this study, we established that chronic exposure of human ASM cells to TAS2R agonists, chloroquine and quinine inhibit human ASM cell survival via Bnip3 up-regulation, DLP-1-mediated mitochondrial fragmentation, and mitochondrial dysfunction (as indicated by decreased mitochondrial membrane potential, cellular ATP levels and increased mitochondrial ROS) leading to initiation of autophagy. Inhibition of mitochondrial fission attenuated the decrease in mitochondrial membrane potential and decreased TAS2R agonists-induced ASM cell death. Further, inhibition of Bnip3 mitochondrial localization by expressing dominant-negative Bnip3 increased human ASM cell survival upon exposure of TAS2R agonists. Our data support a model in which TAS2R agonists inhibit ASM cell survival via Bnip3-mediated mitochondria-dependent mechanism of initiating autophagy (Figure 8).

Autophagy causes proteolytic degradation of cytosolic components. There are three types of autophagy: macro-autophagy, micro-autophagy, and chaperone-mediated autophagy. All these three processes degrade cytosolic components at the lysosomes (38). This is mediated by a special organelle called autophgosome. Autophagic process consists of several sequential steps including sequestration, degradation and amino acid generation. Autophagy is active in most of the cells in the body at basal level to remove damaged organelles and proteins. However, autophagy can also be stimulated in stress situation such as nutrient depletion. During nutrient

shortage, autophagy provides the constituents required for survival. Autophagy is an evolutionary conserved process to maintain the energy balance (30, 32, 44). Recent studies have demonstrated that autophagy plays a role in a variety of physiological and pathological processes besides adaptation to starvation such as development, aging, cancer and muscle disorder (38). Autophagic removal of damaged proteins, organelles including mitochondria, endoplasmic reticulum, peroxisomes serves as an important quality control mechanism for cell survival (16). The regulation of autophagy in mammals is very complicated and involves multiple signaling pathways (5) (41) (7). Dysregulation of autophagy is linked to cell death (9, 33). For example, accumulation of ATGs has been found in mammalian cells undergoing autophagic cell death, which requires the presence of Bcl-2 family proteins (51). Furthermore, excessive autophagy in cells has been shown to induce cell death (9, 33). Our findings in this study demonstrate that chloroquine and quinine mediated cell death in human ASM cells involves autophagy.

Mitochondria are highly dynamic organelles that undergo fission and fusion constantly. Mitochondrial fission and fusion are the key determinants of mitochondria morphology and function (20). Through fission and fusion mechanisms, mitochondria change their length and number. In addition, fission and fusion allow mitochondria to exchange lipid membranes and intra-mitochondrial substance. Such an exchange is essential for maintaining healthy mitochondria population. The shape of the mitochondria is important for the distribution of mitochondria especially in highly polarized cells such as neurons. Excessive mitochondria fission facilitates cell death and the release of inter membrane space substances (31, 56, 57). Mitochondria become elongated when fusion is dominant or fission is insufficient. In contrast, enhanced fission or insufficient fusion causes fragmented mitochondria. A well-balanced fission and fusion is essential for mitochondria health and function. Altered mitochondrial dynamics is

found in human diseases and aging (1, 3, 20, 31, 53, 56, 57). Treatment of human ASM cells with chloroquine and quinine resulted in an increased mitochondrial fission leading to accumulation of fragmented mitochondria and loss of mitochondrial functions.

Mitochondrial fission and fusion are tightly controlled by mitochondrial dynamic machineries. Opa1, Mfn1 and Mfn2 are the key mitochondrial fusion machineries (3, 31). DLP1 is indispensible for mitochondrial fission. DLP1 deletion causes an increase in elongated mitochondria. In contrast, increased mitochondrial DLP1 levels leads to mitochondrial fragmentation (22, 52). Our data support a key role for DLP1 in the regulation of mitochondrial dynamics in response to TAS2R agonist treatment. Increased mitochondrial fragmentation in cells exposed to TAS2R agonists indicates a shift in the balance between fission and fusion likely due to enhanced mitochondrial localization of DLP1. The key role of DLP1-mediated mitochondrial fission in TAS2R agonist-induced cell death was further demonstrated by experiments using DLP1 inhibitor Mdivi-1. Mdivi-1 inhibited TAS2R agonist-induced mitochondrial fission, reversed mitochondrial membrane potential, and attenuated ASM cell death.

In this study, we also demonstrated that TAS2R agonists up regulate expression of Bnip3 and regulate DLP1 translocation to mitochondria. Our data are consistent with recent studies showing that Bnip3 causes DLP1 mitochondrial localization and mitochondrial fragmentation (29). Bnip3 was originally identified as a BH3-only proapoptotic protein of Bcl-2 family inducing mitophagy and mitochondria-mediated cell death. It localizes to the mitochondrial outer membrane and induces mitochondria-initiated cell death through modulation of outer mitochondria membrane permeabilization (26, 48). The expression of Bnip3 is inducible. For example, in cardiac tissues, Bnip3 expression is increased by hypoxia, and up-regulation of

Bnip3 is responsible for ischemia injury-induced cardiomyocyte death (14). Consistent with these findings, our data suggest a role for Bnip3 in TAS2R agonist-induced mitochondrial fragmentation and cell death. Although hypoxia-induced autophagy involves Bnip3, its role in the regulation of cardiomyocyte death is controversial. In an ischemia-reperfusion model, Bnip3-induced autophagy protected myocytes from cell death (18). However, another study showed that Bnip3 promoted autophagic cell death (54). Interestingly, in our study, knocking down Bnip3 partly reversed mitochondrial fragmentation but did not reverse TAS2R agonist-induced ASM cell death (data not shown). This presumably is because cell growth assay requires treatment over 72 h by which time the inhibitory effect of siRNA on Bnip3 expression was diminished. Alternatively, dominant-negative Bnip3, which inhibits Bnip3 mitochondrial localization significantly reversed TAS2R agonist-induced ASM cell death. Our data suggest that in response to TAS2R agonists, increased mitochondrial Bnip3 recruits more DLP1 to mitochondria leading to mitochondrial fragmentation and ASM cell death.

Our previous study demonstrated that the TAS2R agonists, chloroquine and quinine inhibit ASM proliferation induced by FBS, PDGF, or EGF. The anti-mitogenic effects are largely mediated by TAS2R agonist inhibition of cell cycle progression (50). The findings from the current studies demonstrate the role of mitochondria-dependent mechanisms in inhibiting ASM growth by TAS2R agonists. Our data suggest that Bnip3 is a mitochondrial target for the anti-mitogenic effect of TAS2R agonist. Additional studies are needed to determine the relative contribution of multiple cellular mechanisms in mediating anti-mitogenic effect of TAS2R agonists on human ASM cells. Collectively, these studies demonstrate the beneficial effect of TAS2R agonists in mitigating ASM growth, a key component of airway remodeling in asthma

pathogenesis, further underscoring the potential for exploring TAS2Rs as anti-asthma therapeutic targets.

**GRANTS**

This study was supported by grants from American Asthma Foundation and NIH (AG041265) to DAD.

**Footnote**

[#]Current address: Woolcock Institute of Medical Research and School of Life Sciences, University of Technology, Sydney, NSW, Australia, 2007

**DISCLOSURES**

No conflicts of interest, financial or otherwise, are declared by the authors.

**AUTHOR CONTRIBUTIONS**

SP, PS, and SS performed experiments and analyzed data. SP, PS and DD analyzed data, prepared figures and manuscript.

**REFERENCES**


1. Bach D, Pich S, Soriano FX, Vega N, Baumgartner B, Oriola J, Daugaard JR, Lloberas J, Camps M, Zierath JR, Rabasa-Lhoret R, Wallberg-Henriksson H, Laville M, Palacin M, Vidal H, Rivera F, Brand M, Zorzano A. Mitofusin-2 determines mitochondrial network architecture and mitochondrial metabolism. A novel regulatory mechanism altered in obesity. *J Biol Chem* **278**: 17190-17197, 2003.

2. Benayoun L, Druilhe A, Dombret MC, Aubier M, Pretolani M. Airway structural alterations selectively associated with severe asthma. *Am J Respir Crit Care Med* **167**: 1360-1368, 2003.

3. Bereiter-Hahn J. Mitochondrial dynamics in aging and disease. *Prog Mol Biol Transl Sci* **127**: 93-131, 2014.

4. Billington CK, Penn RB. Signaling and regulation of G protein-coupled receptors in airway smooth muscle. *Respir Res* **4**: 2, 2003.

5. Byfield MP, Murray JT, Backer JM. hVps34 is a nutrient-regulated lipid kinase required for activation of p70 S6 kinase. *J Biol Chem* **280**: 33076-33082, 2005.

6. Camoretti-Mercado B. Targeting the airway smooth muscle for asthma treatment. *Transl Res* **154**: 165-174, 2009.

7. Codogno P, Meijer AJ. Autophagy and signaling: their role in cell survival and cell death. *Cell Death Differ* **12 Suppl 2**: 1509-1518, 2005.

8. Dekkers BG, Maarsingh H, Meurs H, Gosens R. Airway structural components drive airway smooth muscle remodeling in asthma. *Proc Am Thorac Soc* **6**: 683-692, 2009.

9. Denton D, Nicolson S, Kumar S. Cell death by autophagy: facts and apparent artefacts. *Cell Death Differ* **19**: 87-95, 2012.

10. Deshpande DA, Penn RB. Targeting G protein-coupled receptor signaling in asthma. *Cell Signal* **18**: 2105-2120, 2006.

11. Deshpande DA, Theriot BS, Penn RB, Walker JK. Beta-arrestins specifically constrain beta2-adrenergic receptor signaling and function in airway smooth muscle. *FASEB J* **22**: 2134-2141, 2008.

12. Deshpande DA, Wang WC, McIlmoyle EL, Robinett KS, Schillinger RM, An SS, Sham JS, Liggett SB. Bitter taste receptors on airway smooth muscle bronchodilate by localized calcium signaling and reverse obstruction. *Nat Med* **16**: 1299-1304, 2010.

13. Dimroth P, Kaim G, Matthey U. Crucial role of the membrane potential for ATP synthesis by F(1)F(o) ATP synthases. *J Exp Biol* **203**: 51-59, 2000.

14. Diwan A, Krenz M, Syed FM, Wansapura J, Ren X, Koesters AG, Li H, Kirshenbaum LA, Hahn HS, Robbins J, Jones WK, Dorn GW. Inhibition of ischemic cardiomyocyte apoptosis through targeted ablation of Bnip3 restrains postinfarction remodeling in mice. *J Clin Invest* **117**: 2825-2833, 2007.

15. Girodet PO, Ozier A, Bara I, Tunon de Lara JM, Marthan R, Berger P. Airway remodeling in asthma: new mechanisms and potential for pharmacological intervention. *Pharmacol Ther* **130**: 325-337, 2011.

16. Glick D, Barth S, Macleod KF. Autophagy: cellular and molecular mechanisms. *J Pathol* **221**: 3-12, 2010.

17. Halwani R, Al-Muhsen S, Hamid Q. Airway remodeling in asthma. *Curr Opin Pharmacol* **10**: 236-245, 2010.

18. Hamacher-Brady A, Brady NR, Logue SE, Sayen MR, Jinno M, Kirshenbaum LA, Gottlieb RA, Gustafsson AB. Response to myocardial ischemia/reperfusion injury involves Bnip3 and autophagy. *Cell Death Differ* **14**: 146-157, 2007.

19. Hassan M, Jo T, Risse PA, Tolloczko B, Lemiere C, Olivenstein R, Hamid Q, Martin JG. Airway smooth muscle remodeling is a dynamic process in severe long-standing asthma. *J Allergy Clin Immunol* **125**: 1037-1045 e1033, 2010.

20. Hesselink MK, Schrauwen-Hinderling V, Schrauwen P. Skeletal muscle mitochondria as a target to prevent or treat type 2 diabetes mellitus. *Nat Rev Endocrinol* **12**: 633-645, 2016.

21. Hornig-Do HT, Gunther G, Bust M, Lehnartz P, Bosio A, Wiesner RJ. Isolation of functional pure mitochondria by superparamagnetic microbeads. *Anal Biochem* **389**: 1-5, 2009.

22. Ikeda Y, Shirakabe A, Maejima Y, Zhai P, Sciarretta S, Toli J, Nomura M, Mihara K, Egashira K, Ohishi M, Abdellatif M, Sadoshima J. Endogenous Drp1 mediates mitochondrial autophagy and protects the heart against energy stress. *Circ Res* **116**: 264-278, 2015.

23. Jheng HF, Tsai PJ, Guo SM, Kuo LH, Chang CS, Su IJ, Chang CR, Tsai YS. Mitochondrial fission contributes to mitochondrial dysfunction and insulin resistance in skeletal muscle. *Mol Cell Biol* **32**: 309-319, 2012.

24. Kaim G, Dimroth P. ATP synthesis by F-type ATP synthase is obligatorily dependent on the transmembrane voltage. *EMBO J* **18**: 4118-4127, 1999.

25. Kaminska M, Foley S, Maghni K, Storness-Bliss C, Coxson H, Ghezzo H, Lemiere C, Olivenstein R, Ernst P, Hamid Q, Martin J. Airway remodeling in subjects with severe asthma with or without chronic persistent airflow obstruction. *J Allergy Clin Immunol* **124**: 45-51 e41-44, 2009.

26. Kubli DA, Ycaza JE, Gustafsson AB. Bnip3 mediates mitochondrial dysfunction and cell death through Bax and Bak. *Biochem J* **405**: 407-415, 2007.

27. Laporte JC, Moore PE, Baraldo S, Jouvin MH, Church TL, Schwartzman IN, Panettieri RA, Jr., Kinet JP, Shore SA. Direct effects of interleukin-13 on signaling pathways for physiological responses in cultured human airway smooth muscle cells. *Am J Respir Crit Care Med* **164**: 141-148, 2001.

28. Laporte JD, Moore PE, Panettieri RA, Moeller W, Heyder J, Shore SA. Prostanoids mediate IL-1beta-induced beta-adrenergic hyporesponsiveness in human airway smooth muscle cells. *Am J Physiol* **275**: L491-501, 1998.

29. Lee Y, Lee HY, Hanna RA, Gustafsson AB. Mitochondrial autophagy by Bnip3 involves Drp1-mediated mitochondrial fission and recruitment of Parkin in cardiac myocytes. *Am J Physiol Heart Circ Physiol* **301**: H1924-1931, 2011.

30. Levine B, Klionsky DJ. Development by self-digestion: molecular mechanisms and biological functions of autophagy. *Dev Cell* **6**: 463-477, 2004.

31. Liesa M, Palacin M, Zorzano A. Mitochondrial dynamics in mammalian health and disease. *Physiol Rev* **89**: 799-845, 2009.

32. Lippai M, Szatmari Z. Autophagy-from molecular mechanisms to clinical relevance. *Cell Biol Toxicol* 2016.

33. Liu Y, Levine B. Autosis and autophagic cell death: the dark side of autophagy. *Cell Death Differ* **22**: 367-376, 2015.

34. Manson ML, Safholm J, Al-Ameri M, Bergman P, Orre AC, Sward K, James A, Dahlen SE, Adner M. Bitter taste receptor agonists mediate relaxation of human and rodent vascular smooth muscle. *Eur J Pharmacol* **740**: 302-311, 2014.

35. Meyerhof W, Batram C, Kuhn C, Brockhoff A, Chudoba E, Bufe B, Appendino G, Behrens M. The molecular receptive ranges of human TAS2R bitter taste receptors. *Chem Senses* **35**: 157-170, 2010.

36. Minet AD, Gaster M. ATP synthesis is impaired in isolated mitochondria from myotubes established from type 2 diabetic subjects. *Biochem Biophys Res Commun* **402**: 70-74, 2010.

37. Misior AM, Yan H, Pascual RM, Deshpande DA, Panettieri RA, Penn RB. Mitogenic effects of cytokines on smooth muscle are critically dependent on protein kinase A and are unmasked by steroids and cyclooxygenase inhibitors. *Mol Pharmacol* **73**: 566-574, 2008.

38. Mizushima N. Autophagy: process and function. *Genes Dev* **21**: 2861-2873, 2007.

39. Moore PE, Lahiri T, Laporte JD, Church T, Panettieri RA, Jr., Shore SA. Selected contribution: synergism between TNF-alpha and IL-1 beta in airway smooth muscle cells: implications for beta-adrenergic responsiveness. *J Appl Physiol (1985)* **91**: 1467-1474, 2001.

40. Moore PE, Laporte JD, Gonzalez S, Moller W, Heyder J, Panettieri RA, Jr., Shore SA. Glucocorticoids ablate IL-1beta-induced beta-adrenergic hyporesponsiveness in human airway smooth muscle cells. *Am J Physiol* **277**: L932-942, 1999.

41. Nobukuni T, Joaquin M, Roccio M, Dann SG, Kim SY, Gulati P, Byfield MP, Backer JM, Natt F, Bos JL, Zwartkruis FJ, Thomas G. Amino acids mediate mTOR/raptor signaling through activation of class 3 phosphatidylinositol 3OH-kinase. *Proc Natl Acad Sci U S A* **102**: 14238-14243, 2005.

42. Pan S, Berk BC. Glutathiolation regulates tumor necrosis factor-alpha-induced caspase-3 cleavage and apoptosis: key role for glutaredoxin in the death pathway. *Circ Res* **100**: 213-219, 2007.

43. Pan S, Wang N, Bisetto S, Yi B, Sheu SS. Downregulation of adenine nucleotide translocator 1 exacerbates tumor necrosis factor-alpha-mediated cardiac inflammatory responses. *Am J Physiol Heart Circ Physiol* **308**: H39-48, 2015.

44. Papandreou ME, Tavernarakis N. Autophagy and the endo/exosomal pathways in health and disease. *Biotechnol J* **12**: 2017.

45. Penn RB, Pronin AN, Benovic JL. Regulation of G protein-coupled receptor kinases. *Trends Cardiovasc Med* **10**: 81-89, 2000.

46. Perkins GA, Sun MG, Frey TG. Chapter 2 Correlated light and electron microscopy/electron tomography of mitochondria in situ. *Methods Enzymol* **456**: 29-52, 2009.

47. Pulkkinen V, Manson ML, Safholm J, Adner M, Dahlen SE. The bitter taste receptor (TAS2R) agonists denatonium and chloroquine display distinct patterns of relaxation of the guinea pig trachea. *Am J Physiol Lung Cell Mol Physiol* **303**: L956-966, 2012.

48. Quinsay MN, Lee Y, Rikka S, Sayen MR, Molkentin JD, Gottlieb RA, Gustafsson AB. Bnip3 mediates permeabilization of mitochondria and release of cytochrome c via a novel mechanism. *J Mol Cell Cardiol* **48**: 1146-1156, 2010.

49. Saxena H, Deshpande DA, Tiegs BC, Yan H, Battafarano RJ, Burrows WM, Damera G, Panettieri RA, Dubose TD, Jr., An SS, Penn RB. The GPCR OGR1 (GPR68) mediates diverse signalling and contraction of airway smooth muscle in response to small reductions in extracellular pH. *Br J Pharmacol* **166**: 981-990, 2012.

50. Sharma P, Panebra A, Pera T, Tiegs BC, Hershfeld A, Kenyon LC, Deshpande DA. Antimitogenic effect of bitter taste receptor agonists on airway smooth muscle cells. *Am J Physiol Lung Cell Mol Physiol* **310**: L365-376, 2016.

51. Shimizu S, Kanaseki T, Mizushima N, Mizuta T, Arakawa-Kobayashi S, Thompson CB, Tsujimoto Y. Role of Bcl-2 family proteins in a non-apoptotic programmed cell death dependent on autophagy genes. *Nat Cell Biol* **6**: 1221-1228, 2004.

52. Shirakabe A, Zhai P, Ikeda Y, Saito T, Maejima Y, Hsu CP, Nomura M, Egashira K, Levine B, Sadoshima J. Drp1-Dependent Mitochondrial Autophagy Plays a Protective Role Against Pressure Overload-Induced Mitochondrial Dysfunction and Heart Failure. *Circulation* **133**: 1249-1263, 2016.

53. Toledo FG, Watkins S, Kelley DE. Changes induced by physical activity and weight loss in the morphology of intermyofibrillar mitochondria in obese men and women. *J Clin Endocrinol Metab* **91**: 3224-3227, 2006.

54. Tracy K, Dibling BC, Spike BT, Knabb JR, Schumacker P, Macleod KF. BNIP3 is an RB/E2F target gene required for hypoxia-induced autophagy. *Mol Cell Biol* **27**: 6229-6242, 2007.

55. Tsurikisawa N, Oshikata C, Tsuburai T, Saito H, Sekiya K, Tanimoto H, Takeichi S, Mitomi H, Akiyama K. Bronchial hyperresponsiveness to histamine correlates with airway remodelling in adults with asthma. *Respir Med* **104**: 1271-1277, 2010.

56. Wang X, Su B, Fujioka H, Zhu X. Dynamin-like protein 1 reduction underlies mitochondrial morphology and distribution abnormalities in fibroblasts from sporadic Alzheimer's disease patients. *Am J Pathol* **173**: 470-482, 2008.

57. Wang X, Su B, Lee HG, Li X, Perry G, Smith MA, Zhu X. Impaired balance of mitochondrial fission and fusion in Alzheimer's disease. *J Neurosci* **29**: 9090-9103, 2009.

58. Yu T, Sheu SS, Robotham JL, Yoon Y. Mitochondrial fission mediates high glucose-induced cell death through elevated production of reactive oxygen species. *Cardiovasc Res* **79**: 341-351, 2008.

**Figure captions**

**Figure 1**. *TAS2R agonists induce human ASM cell death.* Human ASM cells were serum starved for 24 h and then treated with either vehicle or TAS2R agonists (chloro, quin and sacc) at 125 μM in the presence of PDGF (10 ng/ml) for 24 h. **A**. A select set of cells were pretreated with autophagy inhibitors: Baflomycin A (BafA1, 20 nM), and 3-Methyl adenine (3MA, 5μM). A. Cell viability was measured by MTT assay (**$p$<0.01, ***$p$<0.001, n=5). **B**. Light scope images showing cells treated with vehicle control (Con), chloroquine (Chloro), Quinine (Quin), Chloro or Quin+PDGF and cells pre-treated with BafA1 or 3MA before the treatment with PDGF or Chloro or Quin. **C**. A select set of cells were pretreated with either Baf A1, or 3MA before the treatment with PDGF+Chloro or Quin. Cells were stained with anti-LC3 rabbit polyclonal antibody (1:100) followed by FITC-conjugated secondary antibody. Scale bars=20 μm. Representative confocal images are presented (n=4). **D**. Immunoblotting showing results obtained after treating cells either with Chloro or Quin or PDGF alone or Chloro or Quin+PDGF. Key autophagy marker proteins Beclin-1, ATG-5 and LC3β II were found to be increased by treatment with TAS2R agonist in presence of PDGF, results shown are representative of five independent experiments using five human primary ASM cells. **E**. TEM images (6500X mag) showing subcellular structural changes in ASM. Green- Vesicles; Red- autophagosome; Purple-mitochondria. Note accumulation of empty vesicles, double-membrane autophagosomes and deformed mitochondria in cells treated with TAS2R agonist in presence of PDGF. Images shown are representative of n=3 different experiments obtained from three primary human ASM cells.

**Figure 2**. *TAS2R agonists impair mitochondrial function and decrease cellular ATP levels.* Human ASM cells were serum starved for 24 h and then treated with either vehicle or 125 μM TAS2R agonists (chloro and quin) in the absence and presence of 10 ng/ml PDGF (P) for 24 h.

**A**. Mitochondrial membrane potential was measured using TMRE (*$p$<0.05, n=9). **B.** Cellular ATP levels were measured as luciferase intensity (*$p$<0.05, n=3). **C.** Mitochondrial ROS was measured by confocal live-cell imaging using mitoSox red (*$p$<0.05, n=24).

**Figure 3**. *TAS2R agonists increase fragmented mitochondria.* Human ASM cells were serum starved for 24 h and then treated with either vehicle or TAS2R agonists (chloro, quin and sacc) at 125 μM in the absence and presence of 10 ng/ml PDGF (P) for 24 h. **A**. Mitochondria morphology was monitored by confocal live-cell imaging using MitoTracker green. Scale bar=40 μm. **B-C**. Quantitative measurement of mitochondrial morphology using form factor (**B**) and aspect ratio (**C**) after TAS2R agonist treatment (*$p$<0.05, n=5). **D**. Mitochondrial fission protein DLP1, and mitochondrial fusion protein Opa1, Mfn1, and Mfn2 levels were measured by Western blot. Representative blots for DLP1, Opa1, Mfn1 and Mfn2. β-actin was used as a loading control.

**Figure 4**. *TAS2R agonists increase Bnip3 gene expression and DLP1 mitochondrial localization.* Human ASM cells were serum starved for 24 h and then treated with either vehicle or 125 μM TAS2R agonists (chloro and quin) in the absence and presence of 10 ng/ml PDGF (P) for 24 h. **A**. $RT^2$ profiler PCR Array showing mitochondrial gene expression profile. **B**. Bnip3 expression levels after TAS2R agonist treatment (*$p$<0.05, n=4). **C**. Mitochondrial DLP1 and Bnip3 protein levels assayed by Western blot using isolated mitochondrial protein lysates. VDAC was used as internal control for mitochondrial proteins. **D**. Quantified data of **C** showing mitochondrial DLP1 protein levels normalized to VDAC (*$p$<0.05, n=3).

**Figure 5**. *Bnip3 siRNA partly reverses TAS2R agonist-induced mitochondrial fragmentation.* Human ASM cells were transfected with Bnip3 siRNA and then treated with either vehicle or 125 μM TAS2R agonists (chloro, quin, and sacc) in the absence and presence of 10 ng/ml PDGF

(P) for 24 h. **A-B**. Bnip3 siRNA significantly decreased Bnip3 protein levels (*$p$<0.05, n=3). β-actin was used as loading control. **C**. Representative confocal images of MitoTracker labeled mitochondria. Scale bar=50 μm. **D-E**. Quantitative analysis of mitochondria images using form factor (**D**) and aspect ratio (**E**), *$p$ <0.05, n=4.

**Figure 6**. *Dominant-negative Bnip3 inhibits TAS2R agonist-induced human ASM cell death.* Wild type and dominant-negative Bnip3 were transiently expressed in human ASM cells. After serum starvation for 24 h, cells were treated with vehicle, PDGF, or 125 μM TAS2R agonists (chloro or quin) in the presence of 10 ng/ml PDGF (P) for 24 h. GFP and PI positive cells were recorded by confocal imaging. **A**. Representative confocal images indicating the live (GFP positive, green) as well as dead (PI positive, red) cells. **B**. Representative Western blot confirming the successful expression of wild type Bnip3 (WT) and dominant-negative Bnip3 (DN-Bnip3) in human ASM cells. **C**. Human ASM cell survival assay measured by PI staining.

**Figure 7**. *Inhibition of mitochondrial fission by Mdivi-1 increased mitochondrial membrane potential and decreased TAS2R agonist-induced cell death.* Human ASM cells were serum starved for 24 h and pre incubated with either vehicle or 3 μM Mdivi-1 for 2 h. Following the incubation of vehicle or Mdivi-1, cells were treated with vehicle, PDGF, or 125 μM TAS2R agonists (chloro or quin) in the presence of 10 ng/ml PDGF (P) for 24 h. **A**. confocal live-cell imaging showing mitochondrial labeled with MitoTracker Green. **B**. Mitochondrial membrane potential as measured by TMRE fluorescence (n=10 *$p$<0.05). **C**. Representative light scope images of human ASM cells 24 h after treatment. **D**. Human ASM cell viability measured by CyQuant fluorescence (*$p$<0.05; n=3).

**Figure 8**. Proposed mechanisms by which TAS2R agonists induce ASM cell death. TAS2R agonists cause up-regulation of Bnip3 expression followed by increased DLP1 mitochondrial

localization, mitochondrial dysfunction and cell death, which can be attenuated by Mdivi-1 and dominant-negative Bnip3.

Figure 1

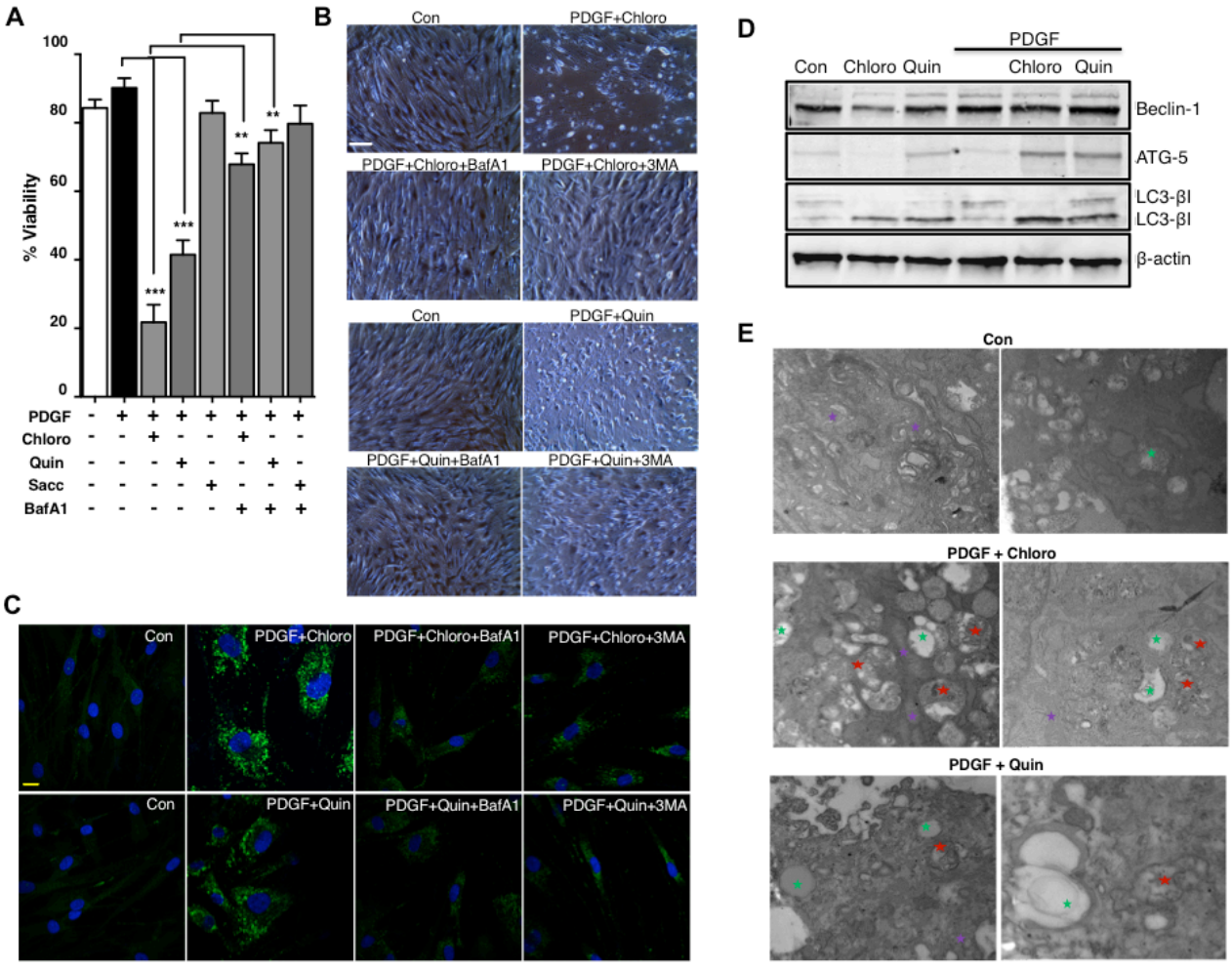
A
100
80
60
40
20
0
% Viability
***
***
**
**
PDGF - + + + + + + +
Chloro - - + - - + - -
Quin - - - + - - + -
Sacc - - - - + - - +
BafA1 - - - - - + + +
B
Con
PDGF+Chloro
PDGF+Chloro+BafA1
PDGF+Chloro+3MA
Con
PDGF+Quin
PDGF+Quin+BafA1
PDGF+Quin+3MA
C
Con
PDGF+Chloro
PDGF+Chloro+BafA1
PDGF+Chloro+3MA
Con
PDGF+Quin
PDGF+Quin+BafA1
PDGF+Quin+3MA
D
PDGF
Con Chloro Quin Chloro Quin
Beclin-1
ATG-5
LC3-βI
LC3-βI
β-actin
E
Con
PDGF + Chloro
PDGF + Quin

Figure 2

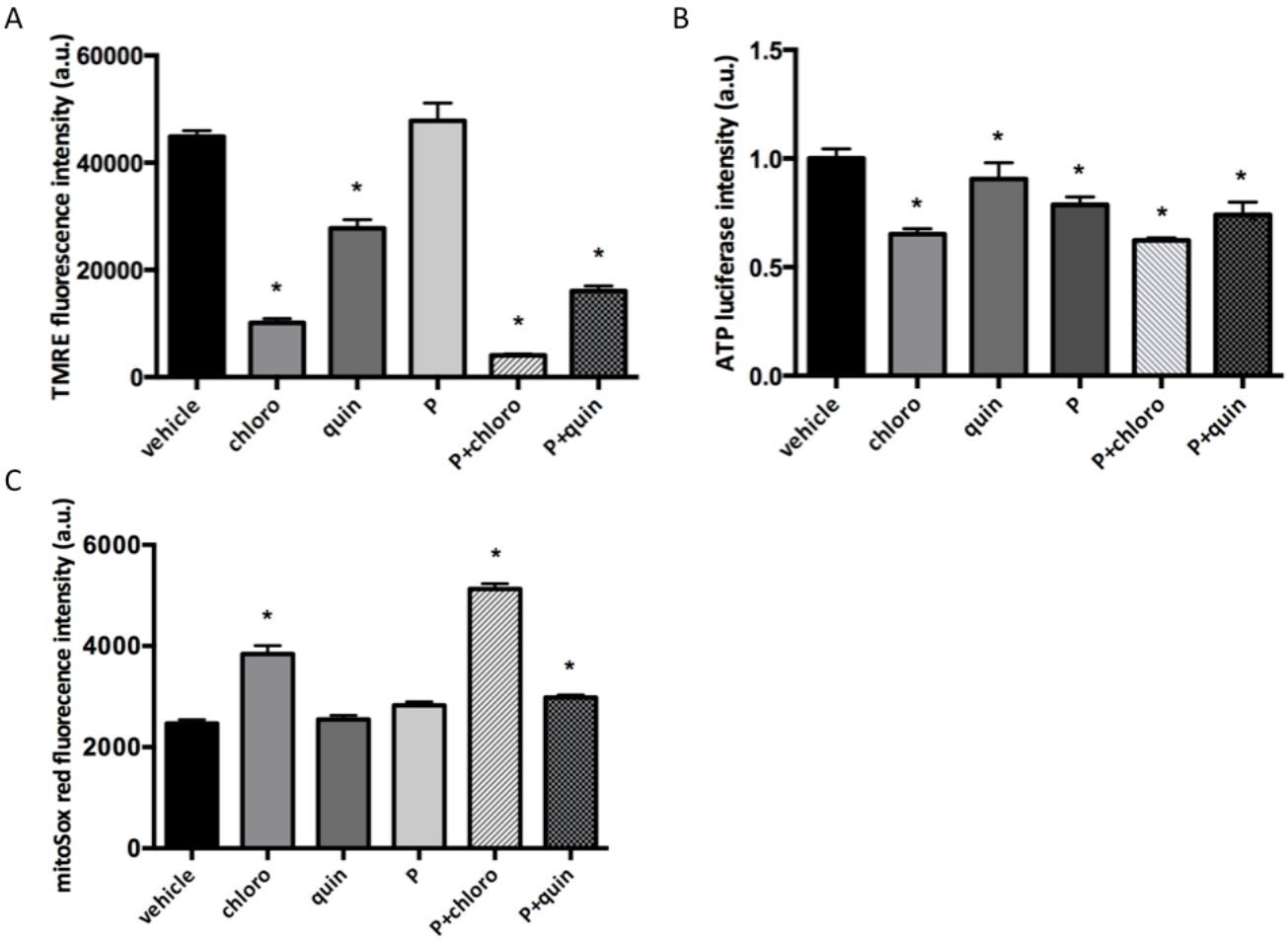
A
TMRE fluorescence intensity (a.u.)
60000
40000
20000
0
vehicle
chloro
quin
P
P+chloro
P+quin
B
ATP luciferase intensity (a.u.)
1.5
1.0
0.5
0.0
C
mitoSox red fluorescence intensity (a.u.)
6000
4000
2000
0

Figure 3

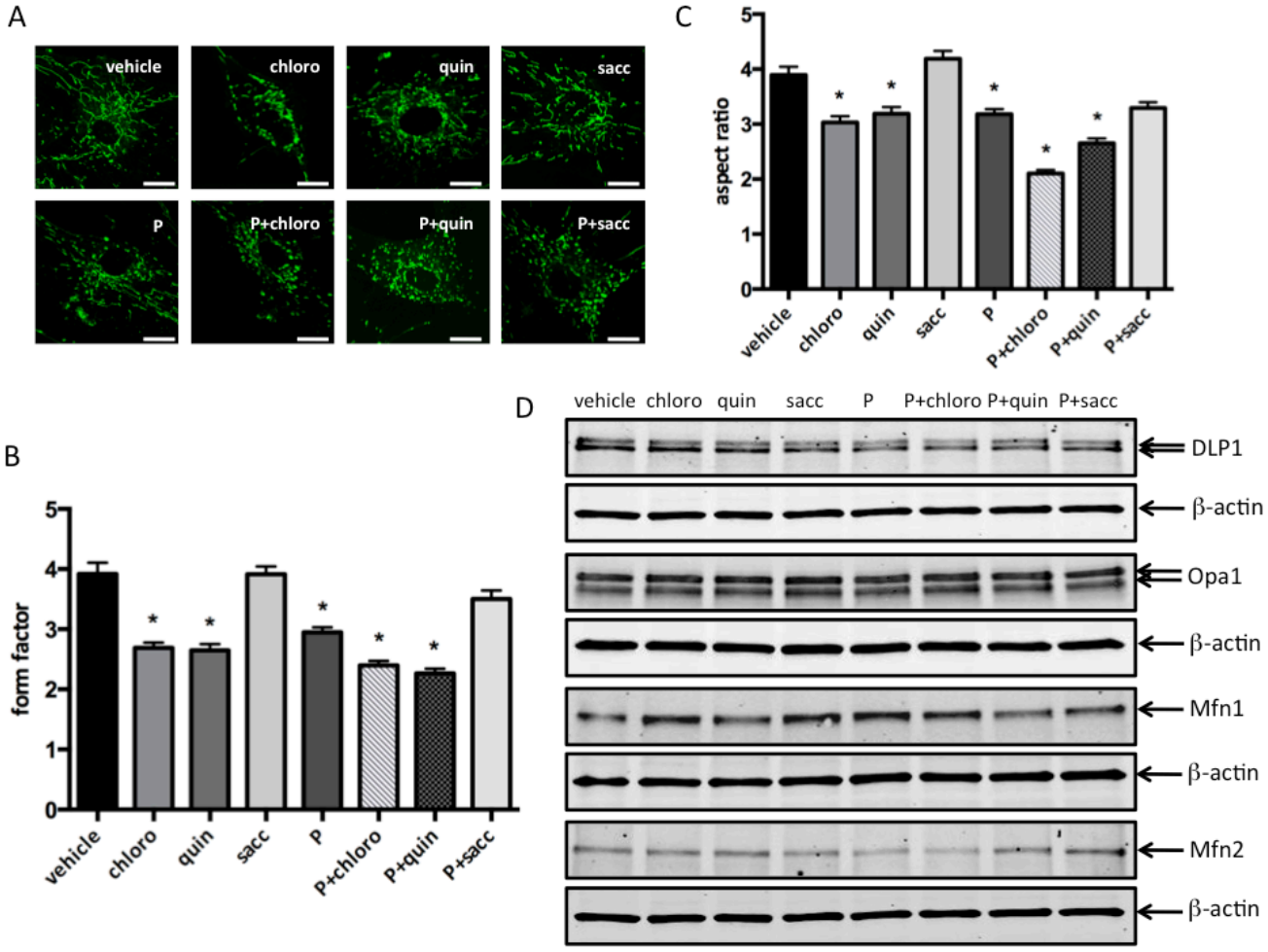
A
vehicle
chloro
quin
sacc
P
P+chloro
P+quin
P+sacc
C
aspect ratio
0
1
2
3
4
5
vehicle
chloro
quin
sacc
P
P+chloro
P+quin
P+sacc
B
form factor
0
1
2
3
4
5
vehicle
chloro
quin
sacc
P
P+chloro
P+quin
P+sacc
D
vehicle
chloro
quin
sacc
P
P+chloro
P+quin
P+sacc
DLP1
β-actin
Opa1
β-actin
Mfn1
β-actin
Mfn2
β-actin

Figure 4

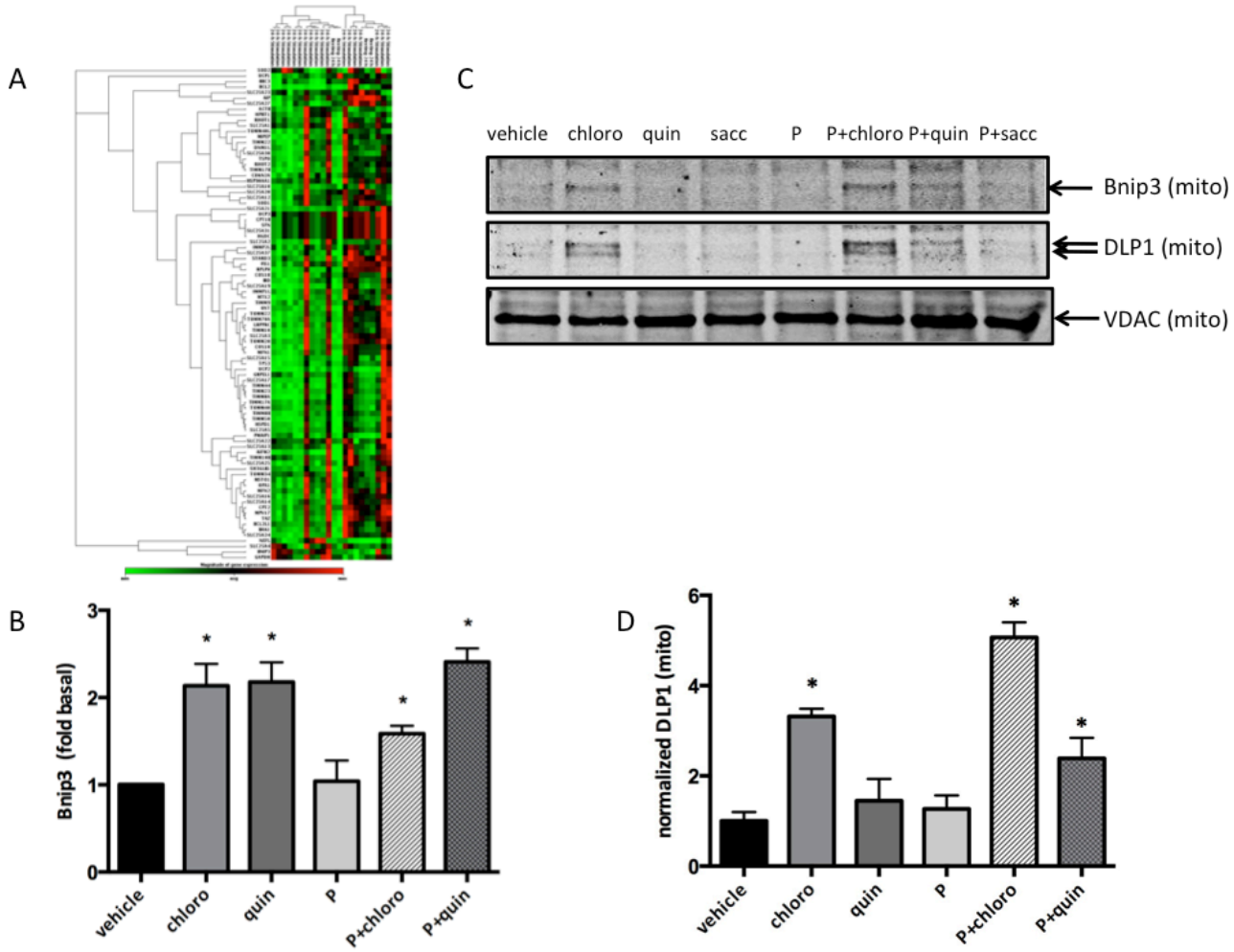
A
C
vehicle
chloro
quin
sacc
P
P+chloro
P+quin
P+sacc
Bnip3 (mito)
DLP1 (mito)
VDAC (mito)
B
Bnip3 (fold basal)
vehicle
chloro
quin
P
P+chloro
P+quin
D
normalized DLP1 (mito)
vehicle
chloro
quin
P
P+chloro
P+quin

Figure 5

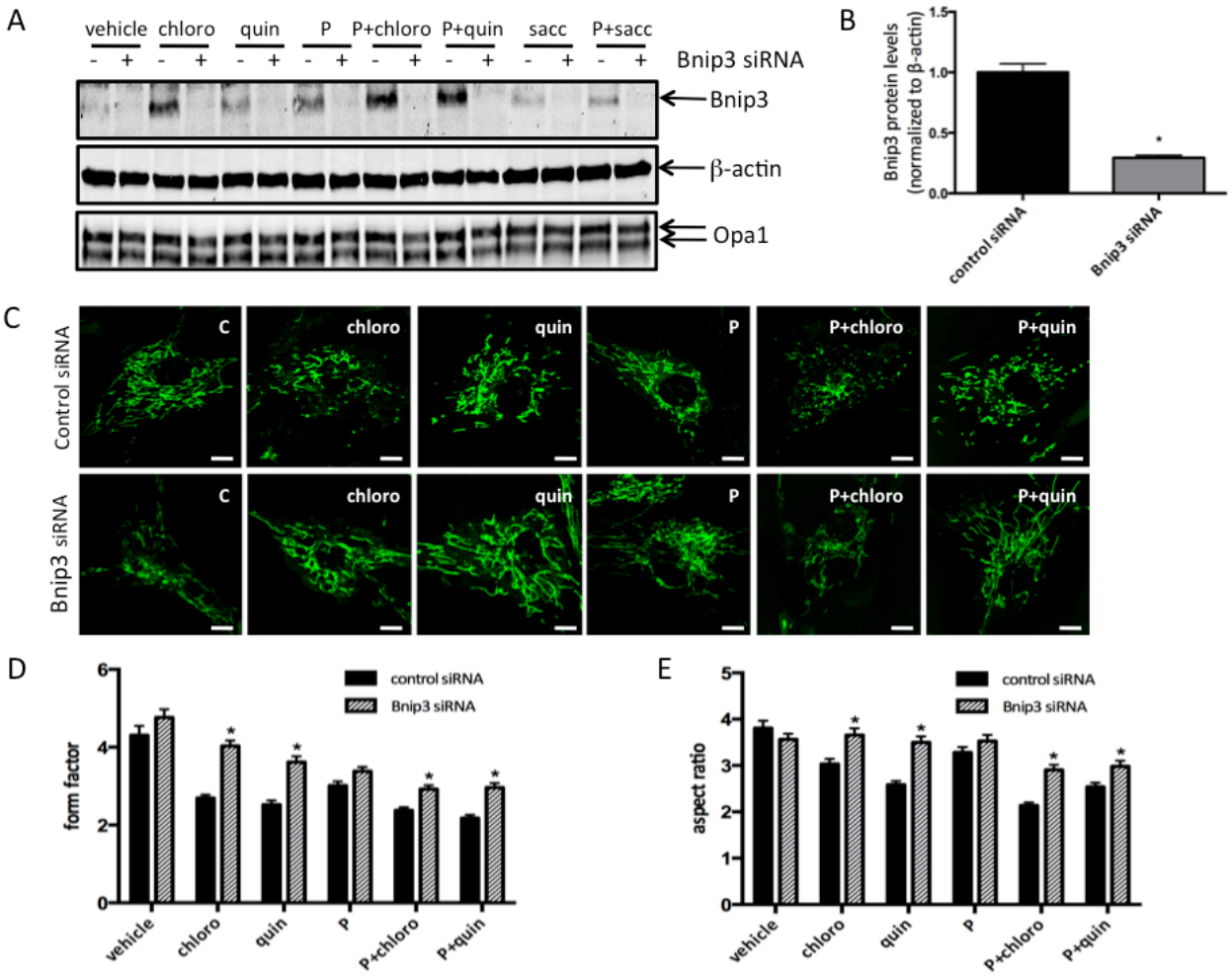
A
vehicle
chloro
quin
P
P+chloro
P+quin
sacc
P+sacc
Bnip3 siRNA
Bnip3
β-actin
Opa1
B
Bnip3 protein levels (normalized to β-actin)
control siRNA
Bnip3 siRNA
C
Control siRNA
Bnip3 siRNA
C
chloro
quin
P
P+chloro
P+quin
D
form factor
control siRNA
Bnip3 siRNA
E
aspect ratio
control siRNA
Bnip3 siRNA

Figure 6

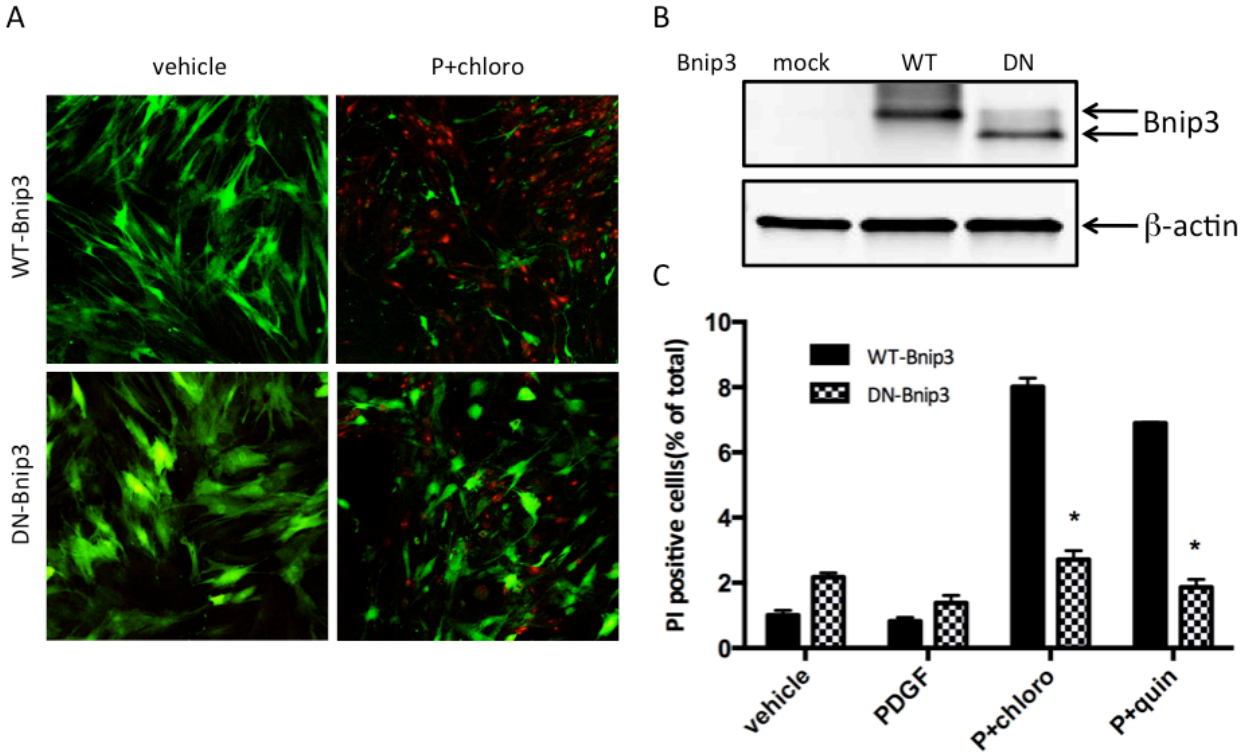
A
vehicle
P+chloro
WT-Bnip3
DN-Bnip3
B
Bnip3
mock
WT
DN
Bnip3
β-actin
C
PI positive cellls(% of total)
WT-Bnip3
DN-Bnip3
0
2
4
6
8
10
*
*
vehicle
PDGF
P+chloro
P+quin

Figure 7

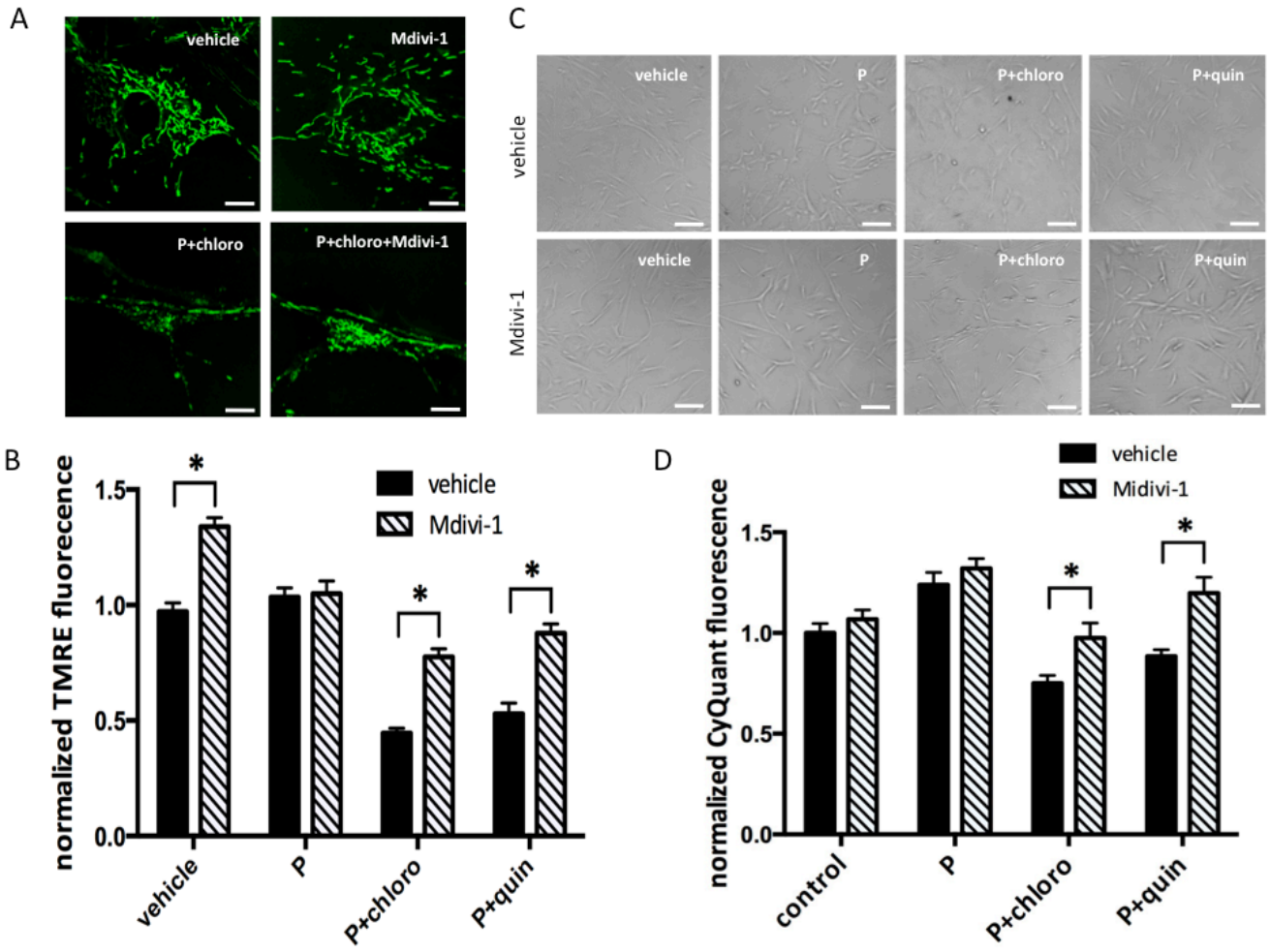
A
vehicle
Mdivi-1
P+chloro
P+chloro+Mdivi-1
C
vehicle
P
P+chloro
P+quin
vehicle
Mdivi-1
B
normalized TMRE fluorecence
vehicle
Mdivi-1
P
P+chloro
P+quin
D
normalized CyQuant fluorescence
vehicle
Midivi-1
control
P
P+chloro
P+quin

Figure 8

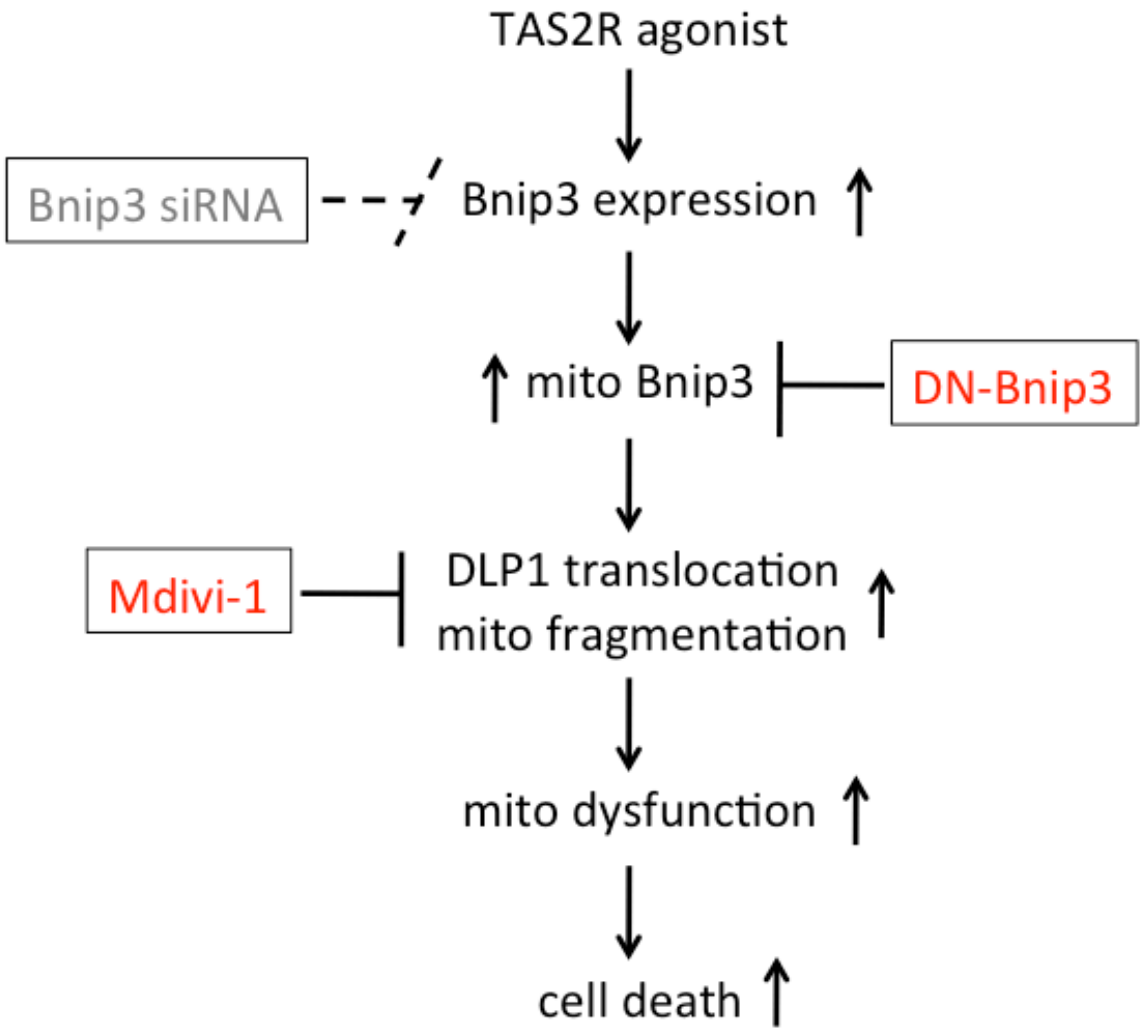
TAS2R agonist
Bnip3 siRNA
Bnip3 expression
mito Bnip3
DN-Bnip3
Mdivi-1
DLP1 translocation
mito fragmentation
mito dysfunction
cell death